THE JOURNAL OF PHYSICAL CHEMISTRY C
A JOURNAL OF THE AMERICAN CHEMICAL SOCIETY

pubs.acs.org/JPCC

Article

Dynamic Disorder Drives Exciton Dynamics in Diketopyrrolopyrrole−Thiophene-Containing Molecular Crystals

Ling Jiang, Jonathan D. Hirst,* and Hainam Do*

Cite This: https://doi.org/10.1021/acs.jpcc.2c07984

Read Online

ACCESS | Metrics & More | Article Recommendations | Supporting Information

ABSTRACT: There is a growing interest in controllable molecular materials for potential nanophotonic and quantum information applications where excitons move beyond the incoherent transport regime. Thus, the ability to identify the key parameters that correlate with the efficiency of the transport of the excitation energy is highly desirable. In this work, we investigate the effects of the dynamic disorder on the transport of the exciton in molecular crystals of several mono- and dialkylated 1,4-diketo-3,6-dithiophenylpyrrolo[3-4-c]pyrrole derivatives. These systems exhibit great potential for photovoltaic applications due to their broad optical absorption and efficient charge transport. The exciton dynamics are studied using a model Hamiltonian, in which the thermal fluctuations of the excitonic coupling (nonlocal electron−phonon coupling), as well as the local exciton−phonon couplings, have been appropriately taken into account. The computed reorganization energies for the most feasible transport pathway ($\pi-\pi$ stacking) for the excitons in UBEQUQ and UBEQOK molecular crystals are 0.366 and 0.357 eV, respectively. These values are comparable with the magnitude of the average excitonic coupling $\langle J \rangle$ ($\approx$ 0.1 eV) for these two molecular crystals. In this instance, the local exciton−phonon coupling is not large enough to form a small exciton-polaron. In addition, substantial coherences are observed on a time scale of less than 100 fs, which indicates that the dynamic disorder is sufficient to overcome quantum dephasing and help drive exciton transport in this class of organic semiconductors. On the other hand, the diffusion of the excitons reduces significantly when the thermal fluctuations of the excitonic coupling are omitted. Thus, dynamic disorder plays a vital role in the transport of the exciton, and the ability to control this inherent property in molecular aggregates will provide valuable tools for the design and development of efficient organic semiconductors.

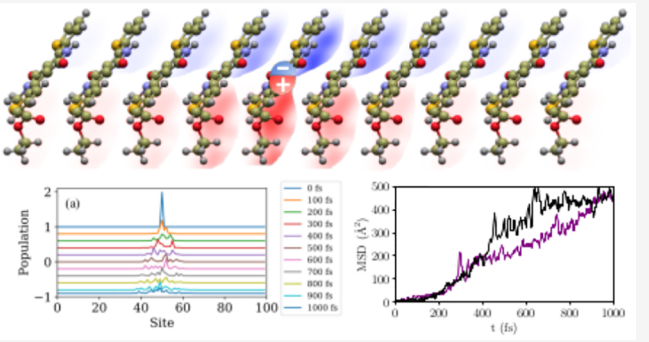

INTRODUCTION

Organic semiconducting materials have the potential to overcome some of the shortcomings associated with inorganic materials and offer new and exciting opportunities for the next generation of electronic devices.[1] These organic molecules contain a wide variety of structures and properties due to the many possible molecular constituents. They could be completely amorphous polymers with interlaced chains, partially ordered polymers, polycrystalline molecules, or molecular crystals.[2,3] Moreover, organic materials can be processed from solution and their electronic properties can be controlled through conventional wet chemistry. Furthermore, they are economical, easily fabricated, biodegradable, and lightweight. Hence, these unique properties make them highly attractive complements to traditional inorganic semiconductors for the development of flexible electronic devices.[4−8]

In recent years, molecular organic semiconductors (OSCs) have been extensively investigated as active components in optoelectronic devices, including organic photovoltaic cells (OPVs) for light-harvesting and power conversion, organic light-emitting diodes (OLEDs) used as light sources, and organic field-effect transistors.[9−14] Thus, efficient exciton diffusion in the active layers (molecular aggregates) over long distances is crucial for the performance of optoelectronic devices. Avoiding the complications that might arise due to defects and grain boundaries, such as exciton trapping and dissociation,[15] the driving force of exciton diffusion is the excitonic coupling (J) between excited states localized on the molecular units. The excitonic coupling can be separated into long-range (Coulombic) and short-range (exchange and overlap) contributions.[16−19] In general, the long-range coupling between the neighboring molecules is the only term

Received: November 14, 2022
Revised: February 10, 2023

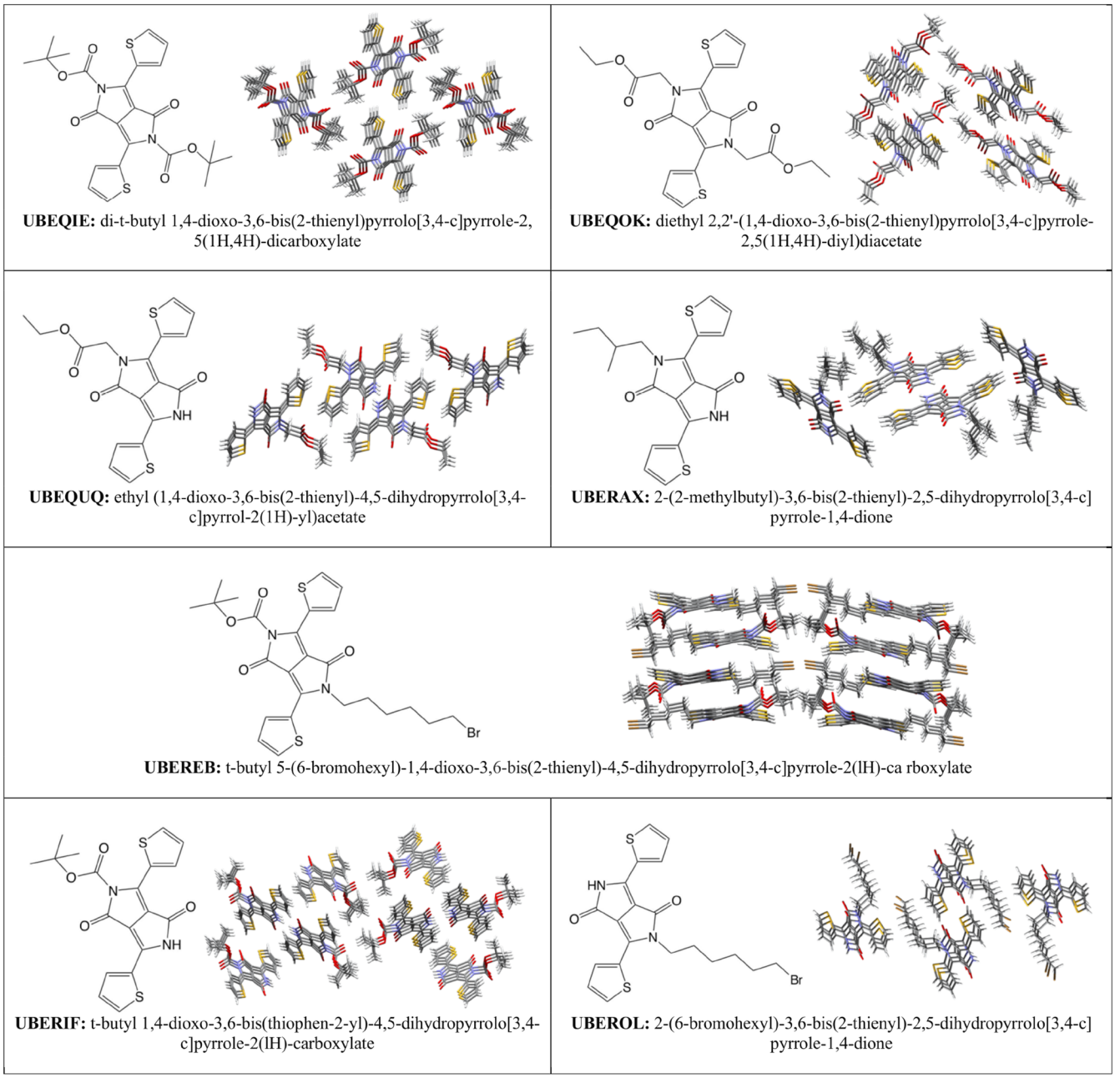

Figure 1. Chemical structures, crystal packing, Cambridge Structural Database codes and names of the studied molecular crystals.

considered for excitation energy transfer in molecular aggregates separated by long intermolecular distances.

On the other hand, the short-range coupling arises mainly from the orbital overlap effect and is crucial for organic molecular crystals whose intermolecular distances are between 3.5 and 5.0 Å.[20,21] In addition, molecular crystals have low-frequency intermolecular vibrations that often cause dynamic disorder (large lattice displacement).[22] The excitonic coupling is sensitive to the relative arrangement of the neighboring molecules. It can fluctuate significantly due to the thermal molecular motions of the system.[21] This phenomenon is referred to as the nonlocal exciton−phonon coupling and plays a vital role in the modulation of exciton transport.[23] Thus, thermal fluctuation of the excitonic couplings must be taken into account for an accurate description of the exciton diffusion in molecular crystals and aggregates with short-range interactions.[24]

Indeed, exciton transport in crystalline organic semiconductors is intrinsically limited by the presence of large thermal molecular motions. These induce localization of the electronic wave function, which survives up to the typical time scales of the intermolecular vibration.[25,26] Generally, these problems are challenging to solve using analytical theory due to the thermal fluctuations and spatial symmetry breaking in the crystal.[27−29] In addition, the nature of excitons in these materials is still not well understood, and a full quantum dynamics treatment is still not accessible due to the size of the systems. Nevertheless, some encouraging progress in characterizing exciton and charge transport has been achieved using mixed-quantum classical molecular dynamics,[30−32] notably the recent work by the Blumberger group using the Frenkel

https://doi.org/10.1021/acs.jpcc.2c07984
J. Phys. Chem. C XXXX, XXX, XXX−XXX

exciton surface hopping approach.[33] Experimental data are invaluable for characterizing the utility of materials for devices, but they often do not give detailed insight into the nature of the exciton transport. Thus, theoretical and computational approaches can be a crucial complement to experiments by providing direct access to microscopic and electronic properties of OSCs and helping to guide their development.

Although coherent transport would be highly desirable in terms of efficiency, exciton diffusion in most molecular materials used for optoelectronic applications takes place via a series of hopping events between neighboring molecules, with exciton diffusion lengths that rarely exceed 100 Å.[34] The coherent regime is less frequent but potentially of great technological importance in the design of efficient exciton transport molecular materials. It is clear now that dynamic disorder is related directly to exciton mobility (coherent regime) in OSCs. More details on the basic physical description of the exciton diffusion in organic semiconductors can be found in the experimental review by Mikhnenko et al.[35] There is growing interest in obtaining controllable molecular materials for nanophotonic and quantum information applications where excitons move beyond the incoherent transport regime.[36,37] In addition, by controlling the amount of dynamic disorder with a suitable mechanical deformation, the performance of molecular films can be significantly improved.[38] These examples demonstrate the importance of dynamic disorder in relation to the design principles for OSC materials. A fundamental understanding of the dynamics of the excitonic coupling and the regime of exciton transport in molecular crystals is a crucial first step in this regard.

Derivatives of small organic molecules such as 1,4-diketopyrrolo[3-4-c]pyrroles (DPPs) have attracted much attention for photovoltaic applications due to their broad optical absorption and efficient charge transport.[39] Moreover, these materials are chemically and thermally stable, are facile to synthesize, and have good solution processability.[40] Thus, DPPs are intensively studied organic building blocks for high-performance pigments[41] and light harvesting chromophores in OSCs.[42] Of the wide variety of chromophores derived from DPP, the series of 1,4-diketo-3,6-dithienylpyrrolo[3-4-c]-pyrroles (TDPP) derivatives is one of the most investigated. These molecules are synthetically accessible and highly planar, resulting in high π-delocalization and favorable $\pi-\pi$ intermolecular interactions.[43] Semiconducting polymers made of these derivatives have attracted much attention due to their excellent hole mobility and high power conversion efficiency, especially when integrated into heterojunction-type polymer solar cells. Although qualitative features of exciton and charge transport in conjugated polymers have long been established, it is still challenging to quantify the structure−property relationships in these materials.[44] Our recent work[45] on these systems has shed some light on this aspect.

Among all the side chains, the alkyl side chain is almost coplanar with the DPP and shows close packing of the molecules,[46] which may enhance the occurrence of singlet exciton fission, allowing high efficiency of OSC devices.[47] Pop et al.[43] synthesized and analyzed the structural and spectroscopic properties of a series of mono- and dialkylated substituted TDPP molecular crystals. They suggested that the ethyl acetate substituents have good potential for modulating and optimizing the charge transport in materials for organic electronic applications, as they promote molecular planarity and close crystal packing (due to the enhancement of the intermolecular hydrogen bonding network). Thus, it is essential to characterize the dynamics of the excitonic coupling in this new class of OSC materials to reveal their exciton transport regimes in the presence of thermal disorder.

In this work, we investigate the exciton transport of these recently synthesized mono- and dialkylated substituted TDPP molecular crystals utilizing computational chemistry tools. First, we employ a force-matching procedure to parametrize new force fields (FFs) for mono- and dialkylated substituted TDPP. In order to mitigate the mismatch in the geometry, the classical potential energy surface and its gradients of the system of interest are mapped onto *ab initio* ones by optimizing the force field parameters. These new FFs are used to propagate the dynamics of the systems, and the equilibrium trajectories (nuclear dynamics) are sampled for electronic structure calculations. After this, the excitonic couplings between all the relevant excited states in the molecular crystal pairs are computed and their fluctuations due to thermal disorder are analyzed. Finally, the exciton dynamics are studied using a Frenkel−Holstein like Hamiltonian with an approximation where the thermal excitonic coupling fluctuations (nonlocal exciton−phonon couplings) have been taken into account.

METHODS

Time-Dependent Model Hamiltonian. The exciton transport of the TDPP molecular crystals we study here can be assumed to take place mainly along the one-dimensional π-stacking columns due to the dominance of their excitonic couplings compared to other intercolumnar excitonic couplings. For example, in the case of UBEQOK (see Figure 1 for the chemical names and structures of the studied molecular crystals), the average coupling value of the π-stacking columns is at least ten times greater than those of other intercolumnar stackings.[48] Similar trends are also observed for other crystals. In addition, as the excitonic coupling between molecular pairs in the π-stacking columns is comparable to the reorganization energy, the coherent transport regime can be invoked (see the Results and Discussion section for more details).[23] Thus, a one-dimensional time-dependent model Hamiltonian that includes all the important physical ingredients can be utilized. This kind of model Hamiltonian is routinely employed to characterize exciton and charge transport in organic semiconducting materials.[23,49,50] Furthermore, in molecular crystals, since the nuclei vibrate at much lower frequencies than the intramolecular and electronic degrees of freedom, we can employ the semiclassical approach to separate the Hamiltonian into a classical part $\hat{H}^{\mathrm{cl}}$ that accounts for the low-frequency nuclear dynamics and a quantum mechanical part $\hat{H}^{\mathrm{qm}}$ that represents the high-frequency degrees of freedom.[23,26,51,52] Thus, the total Hamiltonian of the system is $\hat{H}(t) = \hat{H}^{\mathrm{qm}}(t) + \hat{H}^{\mathrm{cl}}(t)$.

For the quantum mechanical part, we employ a Frenkel−Holstein like Hamiltonian,[26,53,54] which is written as

$$\hat{H}^{\mathrm{qm}}(t) = \sum_{a}^{N}\left(E_{\mathrm{a}} + \sum_{k} g^{(k)} r_a^{(k)}\right)|a\rangle\langle a| + \sum_{a}^{N}\left(J + \sum_{k}\alpha^{(k)}(r_{a+1}^{(k)} - r_a^{(k)})\right)(|a\rangle\langle a+1| + |a+1\rangle\langle a|) \quad (1)$$

https://doi.org/10.1021/acs.jpcc.2c07984
J. Phys. Chem. C XXXX, XXX, XXX−XXX

where a is the index of the molecular site in the one-dimensional aggregate and N is the total number of molecules (sites) in the system. The first sum accounts for the energy of the localized Frenkel excitons, and the second sum describes the excitonic coupling between the nearest neighbors. Localized on each molecule is a single electronic state $|a\rangle$ (in principle, one can consider multiple electronic states) and some harmonic nuclear vibrations (indexed k) with the center of mass displacement $r_a^{(k)}$. E_a is the energy of the lowest singlet excited state, and J is the excitonic couplings between these excited states at adjacent sites. $g^{(k)}$ and $\alpha^{(k)}$ are the local and nonlocal exciton−phonon coupling constants, respectively. When the nuclear modes are in their equilibrium position (i.e., $r_a^{(k)} = 0$), the energy of state $|a\rangle$ is E_a and the excitonic coupling between adjacent states is J.

The exciton−phonon couplings (the time-dependent part of the Hamiltonian) enter the Hamiltonian classically through the time-dependent fluctuations in the atomic coordinates $\mathbf{q}_a^N(t)$. The classical Hamiltonian can be expressed as

$$\hat{H}\mathrm{cl}(t) = \sum_a \frac{\mathbf{p}_a^2}{2m_a} + U(\{\mathbf{q}\}) \tag{2}$$

where $\mathbf{p}_a$ is the momentum conjugate to atomic coordinates $\mathbf{q}_a$, m_a is the mass of particle (atom) a, and $U(\{\mathbf{q}\})$ is the total potential energy of the system. Here, we model these fluctuations using molecular dynamics (MD) simulations of the crystals. Finally, the time-dependent Hamiltonian for a one-dimensional array of molecules is constructed by employing various *ab initio* techniques.

In this model, the nuclear modes couple to the exciton (exciton−phonon coupling) in two different ways. First, the nuclear displacement $r_a^{(k)}$ alters the site energy E_a of the exciton on site a according to the Holstein electron−phonon coupling term $g^{(k)}\ r_a^{(k)}\ |a\rangle\ \langle a|$, where $g^{(k)}$ is the local exciton−phonon coupling constant and is related to the reorganization energy. Second, the nuclear displacements $r_a^{(k)}$ and r_{a+1}^{k} modulate the transfer integral between sites a and a+1 with the term $\alpha^{(k)}(r_{a+1}^{(k)} - r_a^{(k)})$. This is the nonlocal exciton−phonon coupling, and is identified as the main source of the dynamic disorder in molecular aggregates.[53]

Force Field Development. In recent years, MD simulations have found wide applications in the study of the optical and electronic properties of materials and biomolecules, where they are primarily employed to sample the equilibrium structures explored by the system of interest (the nuclear dynamics). These equilibrium trajectories can be utilized in large-scale quantum chemistry calculations to correlate the local structure with the observable electronic structure properties. Consequently, it is vital that the FFs used to describe the nuclear dynamics are accurate enough to capture the true molecular motion of the system. A challenge one often has to confront here is the mismatch in the FFs describing the interactions at the classical level and the electronic structure methods employed for subsequent quantum chemistry calculations. In other words, the potential energy surface of $\hat{H}^{\mathrm{qm}}$ does not coincide with that of $\hat{H}^{\mathrm{cl}}$.

To overcome this challenge, we employ our extension[48] of the adaptive force-matching technique[55] to parametrize the FFs for the studied molecular crystals in this work. The idea behind our procedure is to find a set of parameters that minimizes the differences between the classical forces and the *ab initio* forces. Thus, by design, the FFs used to propagate the nuclear dynamics should be comparable to those targeted *ab initio* methods. In addition, instead of optimizing the parameters for the whole system in one go, which is computationally expensive, we fragment the "larger" molecule into smaller segments, obtain their parameters, and then assemble them together to derive the FFs for the larger molecule. Here, all the studied molecular crystals comprise a DPP core, a thiophene (T) ring, and side chains. Therefore, the building blocks are DPP, T, and the side chains in these cases. The *ab initio* forces (reference forces) are computed using density functional theory (DFT) at the same level of theory as the excitonic coupling and other quantum chemical properties (to mitigate the mismatch in the potential energy surfaces). The long-range-corrected functional ωB97XD is chosen for all quantum chemical calculations because it captures both short- and long-range interactions and describes charge transfer states accurately.[56] All quantum chemistry calculations are performed using the Gaussian 16 package.[57]

For the chromophores, the initial "guessed" parameters are taken from the optimized parameters of DPP, T, and DPP-T in our previous work.[48] For the side chains, we use parameters from the OPLS force field[58] and keep these fixed during the optimization scheme; i.e., we only optimize the parameters for the chromophores and utilize the OPLS parameters for the side chains. We follow the same procedures as in our previous work[48] to obtain a new set of optimized parameters for DPP, T, and DPP-T at the ωB97XD/6-31G* level of theory. Finally, we perform a further optimization for the whole molecule, including side chains, to obtain better sets of parameters. By construction, our FFs are capable of reproducing the potential energy surfaces of those targeted quantum chemical methods.[48] In other words, the sampled nuclear trajectories should be equivalent or very close to those that would have been sampled on the ωB97XD/6-31G* potential energy surface.

Classical MD Simulations of the Crystals. To obtain the nuclear dynamics and evaluate the time fluctuation of the excitonic coupling subject to the thermal motions of the molecular crystals, MD simulations are performed using our new FFs within the NAMD package.[59] As we are interested in the transport of the excitons along the π−π-stacking direction, the supercell of each crystal is created by replicating the unit cell in a way to ensure that there are several hundreds of molecules in the π-stacking columns (to allow for the observation of the exciton diffusion). An example of a supercell of the UBEQUQ is shown in Figure S1.

For all molecular crystals, the systems are minimized using 10000 steepest descent steps followed by 10 ns heating in the NPT ensemble (at 300 K and 1 atm). They are then equilibrated for another 100 ns in the NVT ensemble and continued for another 10 ns in the NVE ensemble for production. The use of three different ensembles helps smoothly bring the systems to the desired conditions (in the NVE ensemble ultimately) without letting the atoms experience unnatural friction from the barostat and the thermostat. Three-dimensional periodic boundary conditions are applied. The Langevin thermostat[60] with a damping coefficient equal to 1 ps^{-1} is employed to keep the temperature constant. The period and decay parameters of the Langevin piston are set to 100 and 50 fs, respectively, to maintain the pressure. A time step of 1 fs for integration of the equations of motion is used throughout the simulations. A cutoff of 12 Å is used for nonbonded interactions. The particle mesh Ewald

https://doi.org/10.1021/acs.jpcc.2c07984
J. Phys. Chem. C XXXX, XXX, XXX−XXX

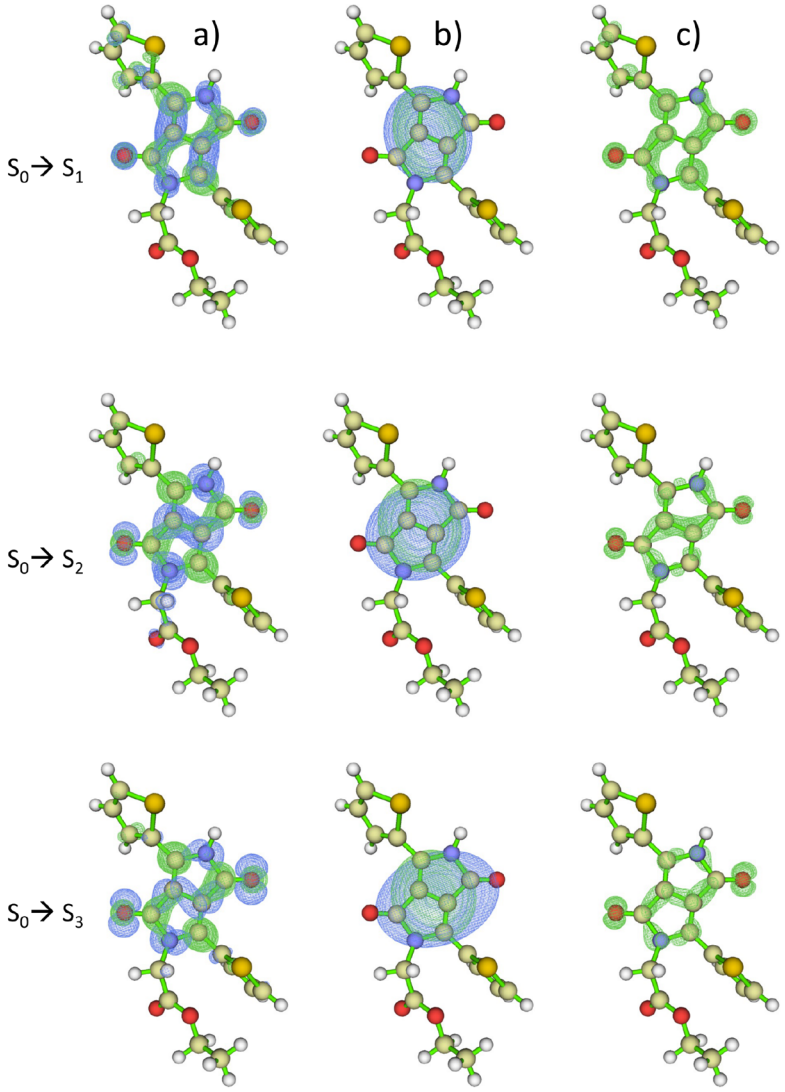

Figure 2. Characterization of the three lowest excited states of an UBEQUQ monomer. (a) Isosurface map of the hole (blue) and electron (green) distribution, (b) isosurface map of the Centroids of the hole and electron, and (c) isosurface map of the overlap of hole and electron.

algorithm[61] is used to calculate long-range electrostatic interactions. To construct the time evolution of the excitonic coupling, nearest neighbors are extracted from 1000 equilibrium MD snapshots, each separated by 50 fs.

Quantum Chemical Calculations. All electronic structure properties, including the excitation energies, transition dipole moments, and atomic transition charges for both the monomers and dimers, are computed using TDDFT at the ωB97XD/6-31G* level of theory. Reorganization energies and Huang−Rhys factors are also computed using the ωB97XD functional but with a larger 6-31** basis set (see Supporting Information (SI) for more details).

Generally, a single-electron excitation is described as the process of an electron leaving the hole. The combination of the hole and the electron (if treated as quasi-particles) is often termed an exciton. For example, in the case of a HOMO → LUMO transition, the hole and the electron could be represented by the HOMO and the LUMO, respectively. This poses a challenge in representing the hole and electron when there is no dominant molecular orbital pair in a transition. In this instance, canonical molecular orbitals are usually transformed into natural transition orbitals. A more robust approach is to define the hole and the electron in terms of their densities (if the phase information is not required).[62] To characterize the electronic excitation of the DPP derivatives, we analyze the electron−hole (e−h) distributions for the lowest three singlet states of both monomer and dimer. Figure 2 indicates that the nature of the lowest three excited states of the monomer is local excitation with the e−h (exciton) both residing on the DPP fragment.

For the case of a dimer, the e−h distributions can either be on a monomer or spread over both molecules, depending on the nature of the excitation. Figure 3 shows that while the $S_0 \rightarrow S_3$ transition is clearly a charge transfer state with the hole staying on monomer 1 and the electron on monomer 2, the two lowest excited states $S_0 \rightarrow S_1$ and $S_0 \rightarrow S_2$ are local excitations (Frenkel excitons). More specifically, the $S_0 \rightarrow S_1$ and $S_0 \rightarrow S_2$ excitons are localized on the DPP fragment on monomers 1 and 2, as shown in Figure 3. Furthermore, the oscillator strengths (f) for the lowest three excited states are 0.219, 0.419, and 0.006, respectively. We also observe the oscillator strengths of the same order of magnitude (or even

https://doi.org/10.1021/acs.jpcc.2c07984
J. Phys. Chem. C XXXX, XXX, XXX−XXX

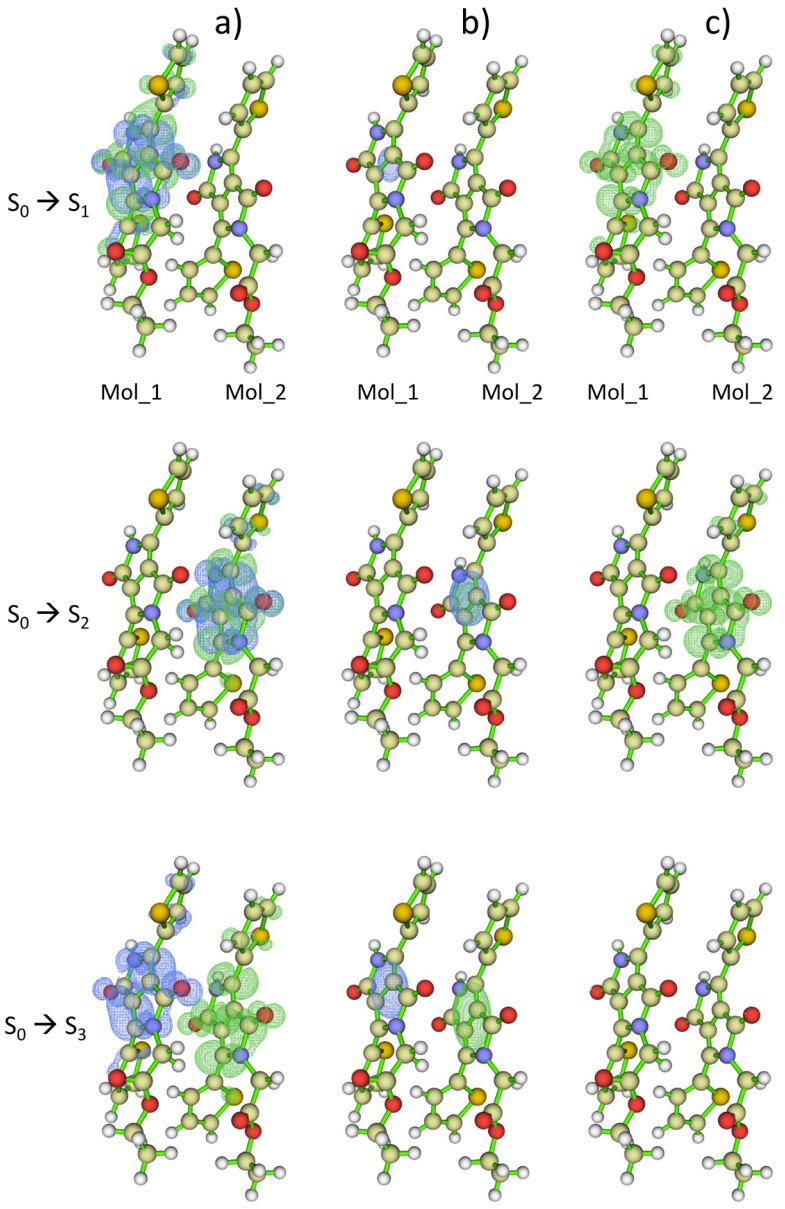

Figure 3. Characterization of the three lowest excited states of an UBEQUQ dimer. (a) isosurface map of the hole (blue) and electron (green) distribution, (b) isosurface map of the Centroids of the hole and electron, and (c) isosurface map of the overlap of hole and electron.

smaller) as that of the $S_0 \rightarrow S_3$ transition for higher excited states. This means that $S_0 \rightarrow S_1$ and $S_0 \rightarrow S_2$ transitions are dominant. Therefore, it is appropriate to neglect the contribution of the charge transfer and higher excited states in an excitation. The exciton can be assumed to be a Frenkel type and reside on a single molecule. Thus, the first two lowest excited states are included in the diabatization process.

For each molecular crystal, the most relevant dimers for the exciton transport are first identified by inspecting the crystal packing. For example, in the case of UBEQUQ (Figure 4), five different relevant dimers (called A, B, C, D, and E) are identified. The excitonic couplings are computed using a diabatization scheme, which is capable of dealing with multiple excited states and also taking into account both short- and long-range effects of the couplings.[21,63] The technique makes use of molecular properties such as transition dipole moments or atomic transition charges to find the best adiabatic-to-diabatic orthogonal transformation matrix **C**, which unitarily

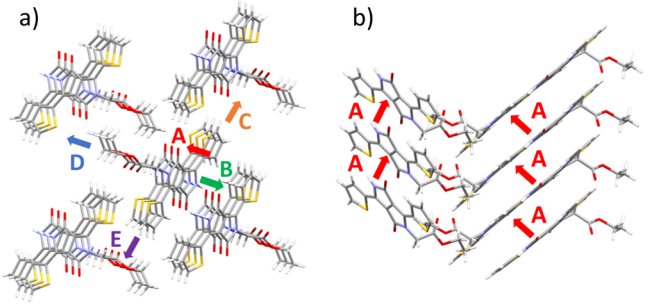

Figure 4. (a) Relevant dimers (coupling pathways A, B, C, D, E) for the exciton transport in UBEQUQ. (b) Coupling pathway A - the parallel π-stacked column.

transforms the adiabatic Hamiltonian matrix $\mathbf{H}^{A}$ to the corresponding diabatic Hamiltonian matrix $\mathbf{H}^{D}$. The diagonal

https://doi.org/10.1021/acs.jpcc.2c07984
J. Phys. Chem. C XXXX, XXX, XXX−XXX

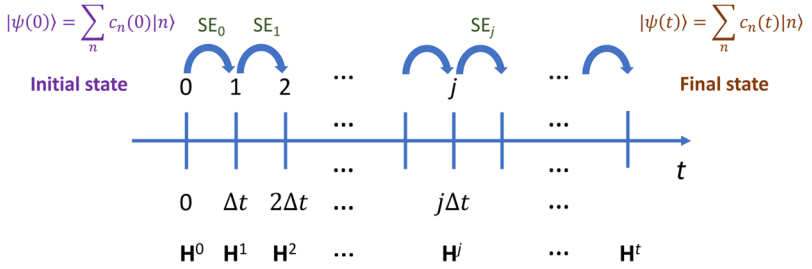

Figure 5. Schematic of the exciton dynamics procedure.

and off-diagonal elements of the diabatic Hamiltonian $\mathbf{H}^{\mathrm{D}}$ are the diabatic energies and excitonic couplings, respectively.

The transition dipole moments and the atomic transition charges can be utilized directly to compute the long-range (Coulombic contributions) excitonic couplings, if the intermolecular interactions of the chromophores are dominated by the electrostatic terms. However, this is not the case for the molecular crystals studied in this work, whose intermolecular distances are relatively short (4 to 5 Å). A comparison of the excitonic couplings computed by using different approaches is shown in Figure S2. The excitonic couplings are computed in vacuum; i.e., the environment polarization effects are not included, as only the Frenkel exciton states are considered. In general, the Frenkel exciton excited states are not sensitive to the relative changes in the dielectric constant in molecular crystals.[23] The polarization effect is only significant for the excitonic coupling between molecules at greater separations and when there is a charge transfer (CT) state.

Exciton Propagation. The exciton dynamics are characterized in a quasi-closed system manner. The nuclear trajectories are classically described, while the exciton propagation is performed in a series of closed quantum system simulations without including energy dissipation or a sink for the exciton. The dynamics disorder is parametrically included in the time-dependent Hamiltonian H(t) via two time-dependent quantities: the nuclear coordinates and the excitonic couplings.

The time evolution of the exciton wave function can be computed by integrating the time-dependent Schrödinger equation (TDSE)

$$i\hbar\frac{\partial}{\partial t}|\psi(t)\rangle = \hat{H}^{\mathrm{qm}}(t)|\psi(t)\rangle \tag{3}$$

where the nuclear dynamics are treated classically. Expanding the exciton wave function $|\psi(t)\rangle$ in terms of the site basis $|a\rangle$ (i.e., $|\psi(t)\rangle = \sum_a c_a(t)|a\rangle$) and multiplying from the left by the complex conjugate basis vector $\langle b|$, eq 3 can be rewritten in terms of matrix elements as

$$i\hbar\frac{\partial c_b(t)}{\partial t} = \sum_a H^{\mathrm{qm}}_{ab}(t)c_a(t) \tag{4}$$

Here, the site basis correspond to an exciton that is localized on a single molecule while the rest are in their ground states.

Equation 4 is solved numerically by updating the time-dependent Hamiltonian $\hat{H}^{\mathrm{qm}}(t)$ discretely every short time interval Δt corresponding to the nuclear dynamics.[64,65] The Hamiltonian is assumed to be constant (time-independent) within each block of time Δt. Thus, for the jth interval, the constant Hamiltonian is $H(t = j\Delta t)$ and labeled as H^j. Therefore, the individual TDSE that needs to be solved is

$$i\hbar\frac{\partial c_b(t)}{\partial t} = \sum_a H^j_{ab}(t)c_a(t) \tag{5}$$

where $t \in [j\Delta t, j\Delta t + \Delta t]$.

The choice of the time step δt is crucial in order to have a stepwise constant Hamiltonian. In other words, each update should introduce a relatively small perturbation to the Hamiltonian from the previous interval. As the relative motions between molecules are much slower than the intramolecular vibrational modes, we choose to update the time-dependent Hamiltonian every 1 fs (i.e., δt = 1 fs). In addition, the root-mean-square displacement (RMSD) of the nuclear coordinates of each molecule in the crystal does not vary significantly within 1 fs. For example, Figures S3 and S4 in the SI show that the RMSDs for UBEQUQ and UBEQOK are only about 0.001 Å. In general, eq 5 can be solved directly by diagonalizing the Hamiltonian matrix $\mathbf{H}^j$ to get the corresponding state basis $|\phi^j_k\rangle$ and hence the time-dependent exciton wave function $|\psi(t)\rangle$. However, to avoid repeatedly diagonalizing the Hamiltonian as well as having to keep changing the basis in each time interval, we instead propagate always in the site basis. We solve each individual TDSE in eq 5 using the master equation solver (zvode) as implemented in the QUTIP package.[66,67] The initial state (wave function) $|\psi(0)\rangle$ is taken to be one of the electronic Hamiltonian eigenstates at t = 0. At the start of the simulation, the initial wave function is projected onto the site basis before the dynamics are propagated. The simulation is performed for 1 ps. A schematic of the algorithm is shown in Figure 5.

The exciton dynamics trajectory is a collection of $|\psi(t)\rangle = \sum_a c_a(t)|a\rangle$ in the site basis, and the exciton population at site a is $|c_a(t)|^2$. Since the environmental effects are taken into account (i.e., thermodynamic ensembles) for the studied systems, it is convenient to work with the density matrices, which also include coherence information. The density matrix $\rho(t)$ for any given wave function $|\psi(t)\rangle$ in the site basis is expressed as

$$\rho(t) = |\psi(t)\rangle\langle\psi(t)| = \sum_{a=1}^{N}\sum_{b=1}^{N}\rho_{ab}(t)|a\rangle\langle b| \tag{6}$$

where the diagonal terms $\rho_{aa}(t)$ give the populations of the exciton on each site a and the off diagonal terms $\rho_{ab}(t)$ describes the coherences between states a and b.

To calculate the average exciton energy, we use the density matrix in the state basis (the eigenstates ϕ^t_k of the Hamiltonian). The density matrix ρ^{ϕ} in the $|\phi^t_k\rangle$ representation is obtained from the density matrix in the site basis $\rho(t)$ as

$$\rho^{\phi}(t) = P^{-1}(t)\rho(t)P(t) = \sum_{k=1}^{N}\sum_{l=1}^{N}\rho^{\phi}_{kl}(t)|\phi^t_k\rangle\langle\phi^t_l| \tag{7}$$

https://doi.org/10.1021/acs.jpcc.2c07984
J. Phys. Chem. C XXXX, XXX, XXX−XXX

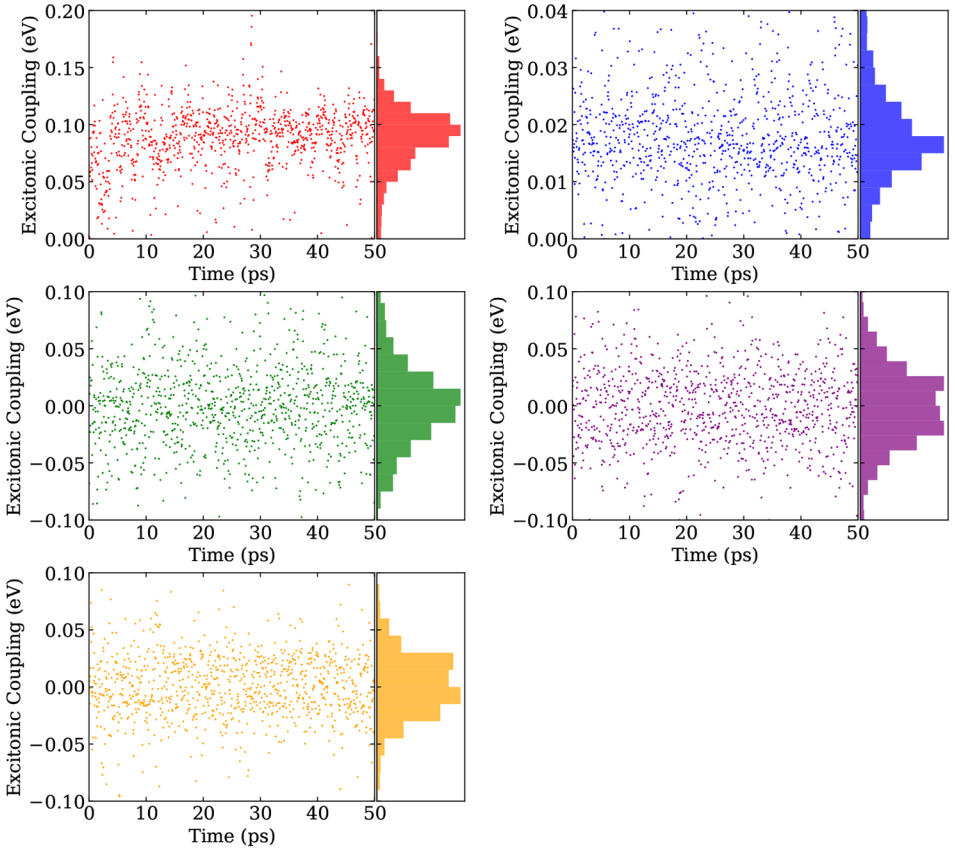

Figure 6. Time evolution and distribution of the excitonic couplings for UBEQUQ computed at 300 K for dimers A, B, C, D, and E, following the definition and color-code in Figure 4.

where $P(t)$ is the projection matrix used to project $\rho(t)$ onto the eigenstate basis. For the j^{th} time interval (i.e., $t \in [j\Delta t, j\Delta t + \Delta t]$) the density matrix $\rho^{\phi}(t)$ is obtained as

$$\rho^{\phi}(t) = P_j^{-1}\rho(t)P_j = \sum_{k=1}^{N}\sum_{l=1}^{N}\rho_{kl}^{\phi}(t)|\phi_k^j\rangle\langle\phi_l^j| \tag{8}$$

where P_j is the projection matrix composed of column vectors for the eigenstates $|\phi_k^j\rangle$. Thus, the average exciton energy $\overline{E}(t)$ for the j^{th} time interval is computed as $\overline{E}(t) = \sum_{k=1}^{N}\rho_{kk}^{\phi}\epsilon_k^j$, where ϵ_k^j is the eigenenergy of the state $|\phi_k^j\rangle$ (i.e., $H^j|\phi_k^j\rangle = \epsilon_k^j|\phi_k^j\rangle$).

RESULTS AND DISCUSSION

Fluctuation of the Excitonic Couplings. To construct the time evolution of the excitonic coupling, nearest neighbors are extracted from 1000 equilibrium MD snapshots each separated by 50 fs. The excitonic couplings for all dimers are computed using TDDFT at the ωB97XD/6-31G* level of theory. Figure 6 shows the time evolution and the distribution of the excitonic couplings computed for the five dimers A, B, C, D, and E for UBEQUQ (see Figure 4). The excitonic couplings are normally distributed. This distribution is also observed for the case of UBEQOK[48] and other studied molecular crystals (Figures S5 to S10). For each system, the largest excitonic coupling is found for the parallel π-stacked dimers, and among all the studied molecular crystals, those π-stacked dimers from UBEQUQ and UBEQOK have the strongest couplings. These results are in accord with the experimental observation[43] that UBEQUQ and UBEQOK have the strongest close packing and $\pi-\pi$ stacking due to their intermolecular hydrogen bonding networks. In general, close packing parallel $\pi-\pi$ stacking enhances excitonic couplings, which is one of the main factors promoting exciton transport in molecular aggregates. Therefore, UBEQUQ and UBEQOK (mono- and dialkyl TDPP based on acetate alkyl units) are postulated to have superior exciton mobility due to the improved close packing.[68] Thus, our aim in this work is to shed light on the experimental observation by characterizing the dynamics of the exciton in these two interesting molecular crystals.

To investigate the characteristic time scale of the fluctuation in the excitonic couplings, Fourier transforms of the autocorrelation functions $\langle\delta J(0)\ \delta J(t)\rangle$, where $J(t)$ is the coupling as a function of time, are computed for dimers in UBEQUQ (Figure 7). Here, the deviation from the average excitonic coupling is defined as $\delta J(t) = J(t) - \langle J(t)\rangle$. Figure 7 shows that low frequency vibrations below roughly 50 cm^{-1} are observed for the π-stacked dimer A. The same trend is also observed for the parallel $\pi-\pi$ stacking in UBEQOK. These low frequency vibrations are believed to be responsible for the large modulation of the excitonic coupling.

Exciton−Phonon Coupling. The reorganization energy (λ) in an exciton transfer process relates directly to the coupling between the electronic and vibrational states in each molecule in the sytem. This coupling is known as the local exciton−phonon coupling and plays a vital role in the modulation of the exciton transport in molecular crystals.[23,51] When the excitonic coupling is significantly smaller than the reorganization energy, the exciton will not have enough

https://doi.org/10.1021/acs.jpcc.2c07984
J. Phys. Chem. C XXXX, XXX, XXX−XXX

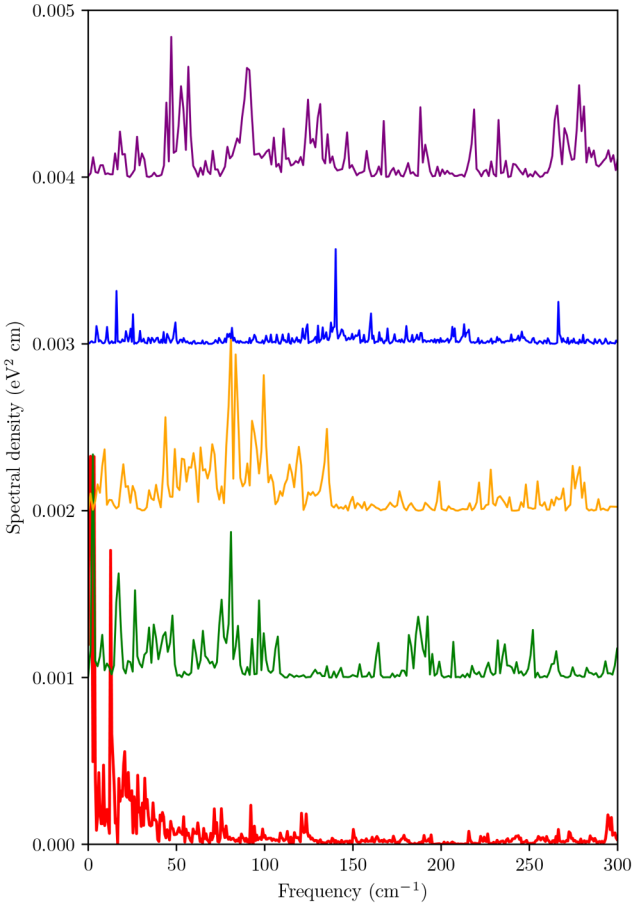

Figure 7. Fourier transformation of the autocorrelation function of the excitonic couplings computed at 300 K for dimers A, B, C, D, and E of UBEQUQ following the definition and color-code in Figure 4.

"energy" to overcome the local exciton−phonon coupling, and therefore will tend to localize on a single site (molecule). In this scenario, the exciton transport will take place in a series of hopping from one site to the others (incoherent or "classical" regime). On the contrary, if the excitonic coupling is comparable or greater than λ, then the exciton is not affected much by the local exciton−phonon coupling, and thus the exciton can be delocalized over many sites. The transport of the exciton in this case will depend largely on the magnitude of the excitonic coupling fluctuation. The total reorganization energies computed for UBEQUQ and UBEQOK ($\pi-\pi$ stacking dimers) are 0.366 and 0.357 eV, respectively. These values are comparable with the magnitude of the average excitonic coupling $\langle J \rangle$ ($\approx$ 0.1 eV) for these two molecular crystals. In addition, when $J > \lambda/4$, which is the case for the two studied molecular crystals, the local exciton−phonon coupling is not large enough to form a small exciton-polaron.[23,69] Thus, we cannot assume, in this case, that the transport of the excitons along the arrays of $\pi-\pi$ stacking molecules in UBEQUQ and UBEQOK is incoherent hopping.

Parameters for the Model Hamiltonian. Referring to the model Hamiltonian shown in eq 1, the set of required parameters is the site excitation energy E_a, the excitonic coupling J between a dimer, the local Holstein exciton−phonon coupling constant g, the nonlocal exciton−phonon coupling constant α, and the nuclear displacement r_a. Here, E_a is set to zero, as each site has the same energy. The constant g is related to the Huang−Rhys factor, which is a unitless number representing the relative shift between two potential energy surfaces (e.g., between the ground state S_0 and the first excited state S_1 potentials). The analysis of the Huang−Rhys factors for UBEQUQ and UBEQOK is described in the SI. For both systems (Figures S14 and S17), only the normal mode at around 1632 cm^{-1} couples strongly with the first electronic transition. These modes are attributed mostly by the stretching of the C−C/C=C bonds, and are responsible for the vibronic progressions often seen in conjugated materials.[50,70,71] Therefore, a single effective vibration can be associated with the total reorganization energy of UBEQUQ and UBEQOK crystals. Following several other studies,[23,26,50,71] we set this effective mode to 1400 cm^{-1} (i.e., $\omega^{(1)}$ = 1400 cm^{-1}) and the mass $m^{(1)}$ = 6 amu (the reduced mass of the C−C/C=C bonds). The local Holstein exciton−phonon constant, for example, for UBEQUQ is calculated as $g^{(1)} = \omega^{(1)}\sqrt{m^{(1)}\lambda}$ = 23 015 cm^{-1} $Å^{-1}$ and the Huang−Rhys factor associated with this effective mode is 0.93.

The instantaneous excitonic coupling J between each pair of dimers (the off-diagonal element) in the time-independent Hamiltonian is randomly drawn from the distribution of the excitonic couplings. Since the Fourier transformation of the autocorrelation function of $J(t)$ (Figure 7) indicates that the low-frequency vibrations (below 50 cm^{-1}) modulate the excitonic coupling in both UBEQUQ and UBEQOK, we set $\omega^{(2)}$ = 25 cm^{-1} as the vibrational frequency of the effective mode that couples strongly to the excitonic coupling. For the effective mass $m^{(2)}$, we use the molecular mass of the crystals. The standard deviation of the excitonic coupling is related to the nonlocal exciton−phonon coupling $\alpha^{(2)}$ as $\sigma_J = \alpha^{(2)}\sqrt{2k_BT/m^{(2)}(\omega^{(2)})^2}$.[23] Table 1 gives the parameters used in our model Hamiltonians.

Table 1. Parameters for the Model Hamiltonian

Parameters	UBEQUQ	UBEQOK	Definition
N	100	100	Number of molecules
$\langle J \rangle$	726 cm^{-1}	645 cm^{-1}	Average excitonic coupling
$g^{(1)}$	23 015 cm^{-1} $Å^{-1}$	22 702 cm^{-1} $Å^{-1}$	Local exciton−phonon coupling constant
$\omega^{(1)}$	1400 cm^{-1}	1400 cm^{-1}	Frequency of mode (1)
$m^{(1)}$	6 amu	6 amu	Effective mass of mode (1)
$\alpha^{(2)}$	1068 cm^{-1} $Å^{-1}$	1091 cm^{-1} $Å^{-1}$	Nonlocal exciton−phonon coupling constant
$\omega^{(2)}$	25 cm^{-1}	25 cm^{-1}	Frequency of mode (2)
$m^{(2)}$	386.44 amu	472.53 amu	Effective mass of mode (2)

Exciton Dynamics. To propagate the dynamics, two time-dependent quantities in the Hamiltonian are required. These are the position of all molecules in the system r_a (nuclear coordinates) and the excitonic coupling J between pairs of molecules. For each set of nuclear arrangements at a time interval, the excitonic coupling must be computed explicitly for each dimer. However, this is prohibitively expensive and is not feasible. Therefore, the standard approach in the literature

https://doi.org/10.1021/acs.jpcc.2c07984
J. Phys. Chem. C XXXX, XXX, XXX−XXX

assumes a fixed value for the excitonic coupling for all pairs of chromophores throughout the simulation. Here, to be more realistic, we draw the excitonic coupling for each dimer at each time step from their statistical distribution dictated by the thermal energy (Figure 6).

Figure 8 shows the time evolution of the exciton wave functions in UBEQUQ and UBEQOK molecular crystals

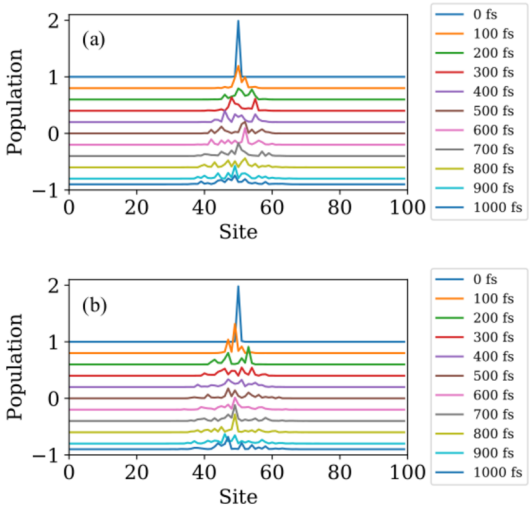

Figure 8. Time evolution of the exciton population for UBEQUQ (a) and UBEQOK (b).

under ambient conditions. In both cases, the exciton is initially localized on a single chromophore at 300 K, and its wave function spreads quickly over the oscillating lattice due to the fluctuation of the excitonic couplings between adjacent molecules (dynamic disorder). Here, the regime of the exciton transport for the studied molecular crystals cannot simply be described by either band or hopping transport. In the band regime the exciton (wave function) is delocalized over the entire system (lattice), whereas in a hopping model the carrier is highly localized and moves by hopping from site to site. Band transport is observed in a perfect crystal, in which a free carrier is delocalized and moves as a plane wave without scattering. However, in real crystals there are always lattice vibrations or phonons that disrupt the crystal symmetry causing the scattering of the electron and reduce its mobility. Band transport can be recovered from the model Hamiltonian (eq 1) by reducing the amount of disorder (e.g., reducing the strength of the nonlocal exciton−phonon couplings). On the other hand, the incoherent hopping regime (small polaron limit) can be obtained by increasing the magnitude of the Holstein local exciton−phonon coupling.

The nature of the nonstationary propagation (variation in the populations and coherences) of the exciton wave function is investigated by examining the evolution of the density matrix $\rho(t)$. As an example, we will discuss the case of the UBEQUQ molecular crystal. The same trend is observed for UBEQOK. Figure 9 shows that starting from the initial pure state at $t = 0$ fs where the exciton is fully localized on a single state, coherence gradually emerges as the exciton gets access to other nearby states. In other words, the exciton mixes from the initial state with other states in a close energy range. The picture becomes clear as time evolves, especially in the later stages when dynamic disorder introduces significant variation to the Hamiltonian. Furthermore, we observe substantial coherences on a time scale of less than 100 fs, which indicates that the dynamic disorder in $H(t)$ is sufficient to overcome quantum dephasing and help drive exciton transport.

Figure 10a shows the thermal fluctuations of the average exciton energies for UBEQUQ and UBEQOK at 300 K. The data indicate that the excitons in both systems are in thermal equilibrium throughout the 1 ps simulation time. The total average exciton energies are 1.0 and 1.1 eV for UBEQUQ and UBEQOK, respectively. These values are within the same range as those for other organic materials such as oligoacene.[72−74]

To characterize the diffusion of the exciton, we compute the temporal evolution of the mean-square-displacement (MSD) of the center of the exciton (x_a) in real space. Here, the MSD is defined as $(\overline{x}(t) - \overline{x}(0))^2$, where $\overline{x}(t) = \sum_a^N \rho_{aa}\, x_a(t)$. Figure 10b shows that the MSDs of the exciton in both UBEQUQ and UBEQOK vary approximately linearly with time (normal diffusion) and there is still free diffusion for the exciton beyond 1 ps. Since the average excitonic coupling of UBEQUQ is greater than that of UBEQOK, we can expect that the exciton diffuses faster (larger MSD values) in UBEQUQ, which is what is observed in Figure 10b. Using the one-dimensional diffusion equation ($\mathrm{MSD}(t) = 2Dt$), we can extract the diffusion coefficient D from the gradients of the MSD plots. From these

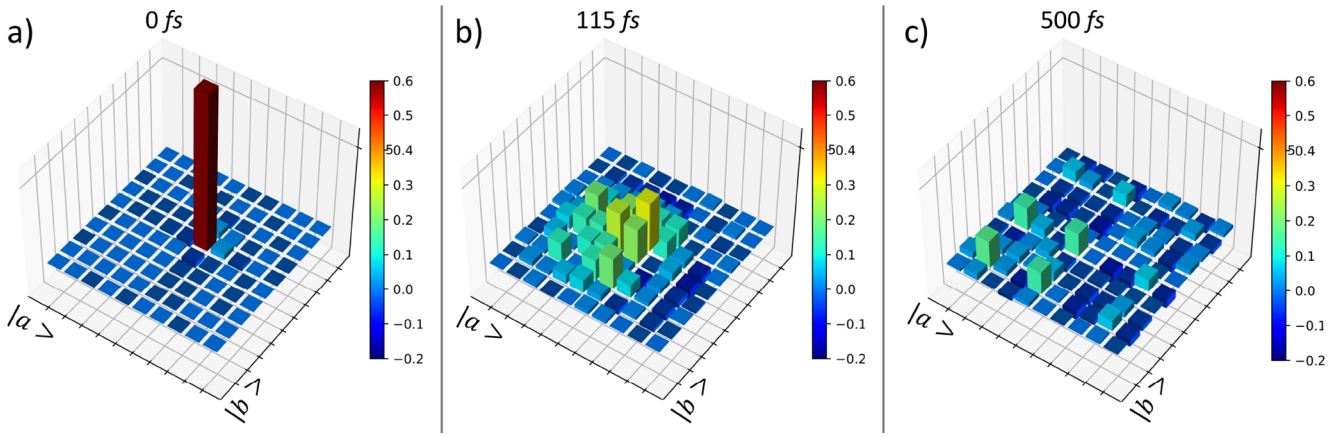

Figure 9. Snapshots of the evolution of the density matrix of UBEQUQ at (a) $t = 0$ fs, (b) $t = 115$ fs, and (c) $t = 900$ fs. Only states with significant populations are included.

https://doi.org/10.1021/acs.jpcc.2c07984
J. Phys. Chem. C XXXX, XXX, XXX−XXX

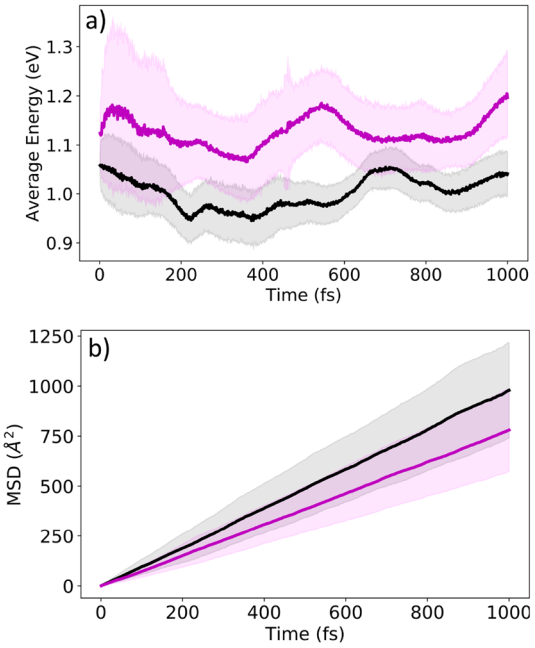

Figure 10. (a) Average energy $\bar{E}(t)$ of the exciton computed for UBEQUQ (black) and UBEQOK (magenta). (b) Time evolution of the mean-square-displacement of the center of the exciton for UBEQUQ (black solid line) and UBEQOK (magenta solid line). The shaded areas indicate the standard deviations.

measurements, diffusivity values of ∼0.1 $cm^2\ s^{-1}$ and ∼0.08 $cm^2\ s^{-1}$ are found for UBEQUQ and UBEQOK, respectively. These values are within the same order of magnitude as those computed for other molecular crystals[23,51] and a recently measured diffusion coefficient for metal-halide perovskites.[75]

Since decoherence correction in the exciton dynamics is not included in our propagation approach, the wave function may progressively overpopulate high energy states, unphysically heating up the system in the long-time limit. These effects have been thoroughly investigated in recent studies by Carof et al.[76] and Xie et al.[77] for anthracene crystals. Under this condition, diffusion coefficients may be overestimated, and convergence of the diffusion with system size may not be reached.[76] Nonetheless, the time scale of our simulations is relatively short (<1 ps). We suspect that these effects do not significantly affect the results of our diffusion coefficients.

To quantify the evolution of the exciton, we compute the survival probability $P_S(t)$ of the initial state defined as $|\langle\psi(0)|\psi(t)\rangle|^2$, which is essentially the square of the overlap integral between the initial wave function and the wave function at time t. Here, the initial state $|\psi(0)\rangle$ is chosen to have an exited molecule in the middle of the stack while others are in their ground states. In addition, to characterize the enhancement of the exciton transport by dynamic disorder, we also calculate the survival probability of the exciton for two other cases: (i) a fully "static" Hamiltonian (both nuclear coordinates and excitonic couplings are fixed) and (ii) a partial "static" Hamiltonian with constant excitonic couplings (nuclear coordinates are updated). Here, we choose to use H^1 as the initial starting Hamiltonian. Figure 11a shows that, for the case of the fully "static" Hamiltonian H^1 of UBEQUQ, the exciton does not evolve significantly from the initial state after 1 ps, while, for the dynamic case, $H(t)$, the overlap decreases quickly and reaches about 0 at 1 ps. The oscillatory behavior of the survival probability observed for the case of the static Hamiltonian H^1 indicates that H^1 remains in the pure state (no environmental effects). In other words, H^1 is in a coherent superposition of the basis states. The sharp fall in $P_S(t)$ of the time-dependent Hamiltonian $H(t)$ between 0 to 400 fs demonstrates the role of the dynamic disorder in the transport of excitons. The original pure state H^0, which is stationary with no coherence between exciton states, is transformed into a

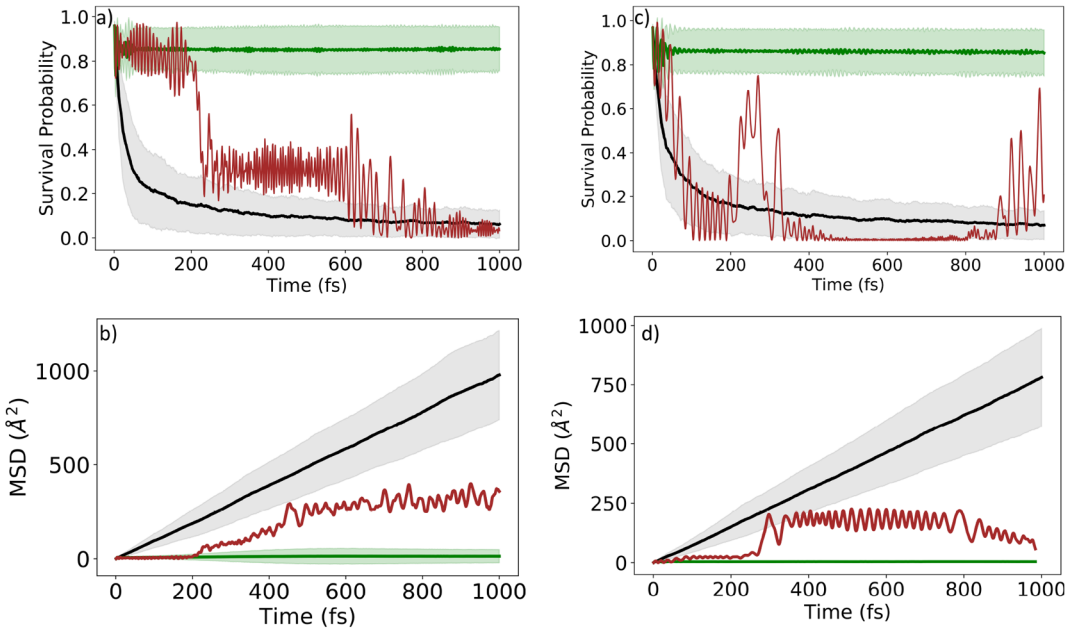

Figure 11. Survival probability P_S of the initial state of UBEQUQ (a) and UBEQOK (c), and time evolution of the mean-square-displacement of the center of the exciton of UBEQUQ (b) and UBEQOK (d) in the case of the time-dependent Hamiltonian $H(t)$ (black solid line), static Hamiltonian H_1 (green solid line), and constant coupling J (brown solid line). The shaded areas indicate the standard deviations. For the case of constant J, error bars are relatively small and not visible from the plot.

https://doi.org/10.1021/acs.jpcc.2c07984
J. Phys. Chem. C XXXX, XXX, XXX−XXX

mixed state due to the evolution of the Hamiltonian. Each update of the time-dependent Hamiltonian $H(t)$ disturbs the coherent evolution in the previous period and at the same time it introduces new coherences.[78,79] This indicates the complex nature of the exciton transport in such a coherent regime.[80]

In the third case, when the fluctuation in the excitonic coupling is not taken into account, i.e. the coupling J is fixed at its average value, the dynamics of the exciton are altered significantly compared to the case of the time-dependent Hamiltonian $H(t)$ (Figure 11a and 11b). The wave function is still significantly overlapped with the initial states after 1 ps, and the exciton mobility substantially reduces. The same trend is also obtained for UBEQOK (Figure 11c and 11d). In addition, the oscillatory behavior of the survival probability observed in this case also somewhat indicates the "static" nature of the Hamiltonian. Thus, these results confirm the crucial role of the dynamic disorder of the excitonic couplings, and a simple average constant value often employed in the literature may not be adequate to fully describe the exciton transport in molecular aggregates.

CONCLUSION AND OUTLOOK

Dynamic disorder is the key property that drives the excitation energy transfer in molecular crystals and is a valuable tool for the design and development of efficient organic semiconductors. In this work, we present a systematic computational procedure to characterize the dynamics of the exciton in molecular crystals. We apply our approach to understand the excitation energy transfer in a recently synthesized class of molecular crystals containing diketopyrrolopyrrole and thiophene groups. Derivatives of these small organic molecules have attracted much attention for photovoltaic applications due to their broad optical absorption and efficient charge transport.

Out of all the studied molecular crystals, the π-stacked parallel columns of UBEQUQ and UBEQOK possess the strongest excitonic couplings and also exhibit a significant fluctuation in the excitonic couplings due to the low-frequency intermolecular vibrations between 10 to 50 cm^{-1}. This is attributed directly to the closed packing nature and the geometry of the aromatic core (which is strongly influenced by the side substituent) of the two crystals. The excitonic couplings are normally distributed. Given the strength of the couplings in these systems, the exciton transport is assumed to occur in the coherent regime, in which the fluctuations of the excitonic couplings first induce the localization of the exciton wave function. Subsequently, with the aid of the low-frequency modes that modulate the excitonic couplings, the exciton wave function spreads rapidly over neighboring lattices.

The fluctuation of the excitonic couplings (dynamic disorder) is vital for the exciton transport in molecular crystals. In particular, the common approach of utilizing a fixed average value for the excitonic coupling J for all pairs of chromophores in the model Hamiltonian seems not to be adequate. In theory, the coupling should be computed separately for each dimer in the system at each time step along the exciton trajectories. In addition, many-body effects, i.e., beyond nearest-neighbor couplings, should also be considered. For example, the accumulation of all extended interactions may be comparable to the magnitude of the nearest-neighbor couplings. This effect is particularly important for less ordered materials, such as polycrystalline, semicrystalline, or amorphous states, in which the nature of the exciton transport is three-dimensional. However, this is prohibitively expensive in practice and is not accessible with current computing power. Nevertheless, to be more realistic, the excitonic couplings for each pair of dimers should be drawn from their statistical distribution that is dictated by the thermal energy. Alternatively, the excitonic couplings can also be taken from a coupling map or machine learned values and these approaches will be pursued in our future work to obtain a better description of the transport mechanism of the exciton in molecular aggregates.

ASSOCIATED CONTENT

Supporting Information

The Supporting Information is available free of charge at https://pubs.acs.org/doi/10.1021/acs.jpcc.2c07984.

Chemical names and structures of the studied molecular crystals; reorganization energy and Huang–Rhys factor calculations (PDF)

AUTHOR INFORMATION

Corresponding Authors

Jonathan D. Hirst − *School of Chemistry, University of Nottingham, Nottingham NG7 2RD, U.K.;* orcid.org/0000-0002-2726-0983; Email: jonathan.hirst@nottingham.ac.uk

Hainam Do − *Department of Chemical and Environmental Engineering and Key Laboratory of Carbonaceous Waste Processing and Process Intensification Research of Zhejiang Province, University of Nottingham Ningbo China, Ningbo 315100, China; New Materials Institute, University of Nottingham Ningbo China, Ningbo 315042, China;* orcid.org/0000-0003-4239-6157; Email: hainam.do@nottingham.edu.cn

Author

Ling Jiang − *Institute of Bioengineering, College of Chemical and Biological Engineering, Zhejiang University, Hangzhou, Zhejiang 310027, China; ZJU-Hangzhou Global Scientific and Technological Innovation Centre, Hangzhou, Zhejiang 311200, China*

Complete contact information is available at: https://pubs.acs.org/10.1021/acs.jpcc.2c07984

Notes

The authors declare no competing financial interest.

ACKNOWLEDGMENTS

We are grateful for access to the University of Nottingham High Performance Computing Facility both in Ningbo China and Nottingham UK. L.J. thanks the Faculty of Science and Engineering at University of Nottingham Ningbo China for a PhD scholarship. H.D. is supported by The Research Fund for International Young Scientists (Grant No. 21850410456). This work is financially supported by the National Natural Science of China (Grant Nos. 21875106 and 22171153). J.D.H. is supported by the Royal Academy of Engineering under the Chairs in Emerging Technologies scheme. The Zhejiang Provincial Department of Science and Technology is acknowledged for this research under its Provincial Key Laboratory Programme (2020E10018).

DEDICATION

Dedicated to the memory to our dear friend and colleague, Professor Nick Besley.

REFERENCES

(1) Forrest, S. R. Electronic Appliances on Plastic. *Nature* **2004**, *428*, 911−918.
(2) Rivnay, J.; Mannsfeld, S. C.; Miller, C. E.; Salleo, A.; Toney, M. F. Quantitative determination of organic semiconductor microstructure from the molecular to device scale. *Chem. Rev.* **2012**, *112*, 5488−5519.
(3) Noriega, R.; Salleo, A.; Spakowitz, A. J. Chain conformations dictate multiscale charge transport phenomena in disordered semiconducting polymers. *Proc. Natl. Acad. Sci. U. S. A.* **2013**, *110*, 16315−16320.
(4) Moorthy, S. B. K. *Thin film structures in energy applications*; Springer: Cham, 2015.
(5) Dantanarayana, V.; Nematiaram, T.; Vong, D.; Anthony, J. E.; Troisi, A.; Nguyen Cong, K.; Goldman, N.; Faller, R.; Moulé, A. J. Predictive Model of Charge Mobilities in Organic Semiconductor Small Molecules with Force-Matched Potentials. *J. Chem. Theory Comput.* **2020**, *16*, 3494−3503.
(6) Liu, Y.; Chen, C.-C.; Hong, Z.; Gao, J.; Yang, Y. M.; Zhou, H.; Dou, L.; Li, G.; Yang, Y. Solution-processed small-molecule solar cells: breaking the 10% power conversion efficiency. *Sci. Rep.* **2013**, *3*, 1−8.
(7) Meredith, P.; Armin, A. Scaling of next generation solution processed organic and perovskite solar cells. *Nat. Commun.* **2018**, *9*, 8−11.
(8) Patel, B. B.; Diao, Y. Multiscale assembly of solution-processed organic electronics: the critical roles of confinement, fluid flow, and interfaces. *Nanotechnology* **2018**, *29*, 044004.
(9) Schweicher, G.; Garbay, G.; Jouclas, R.; Vibert, F.; Devaux, F.; Geerts, Y. H. Molecular Semiconductors for Logic Operations: Dead-End or Bright Future? *Adv. Mater.* **2020**, *32*, 1905909.
(10) Dou, L.; You, J.; Hong, Z.; Xu, Z.; Li, G.; Street, R. A.; Yang, Y. 25th anniversary article: a decade of organic/polymeric photovoltaic research. *Adv. Mater.* **2013**, *25*, 6642−6671.
(11) Sirringhaus, H. 25th anniversary article: Organic field-effect transistors: The path beyond amorphous silicon. *Adv. Mater.* **2014**, *26*, 1319−1335.
(12) Lin, P.; Yan, F. Organic thin-film transistors for chemical and biological sensing. *Adv. Mater.* **2012**, *24*, 34−51.
(13) Jou, J.-H.; Kumar, S.; Agrawal, A.; Li, T.-H.; Sahoo, S. Approaches for fabricating high efficiency organic light emitting diodes. *J. Mater. Chem. C* **2015**, *3*, 2974−3002.
(14) Krämer, M.; Dohmen, P. M.; Xie, W.; Holub, D.; Christensen, A. S.; Elstner, M. Charge and Exciton Transfer Simulations Using Machine-Learned Hamiltonians. *J. Chem. Theory Comput.* **2020**, *16*, 4061−4070.
(15) Chen, K.; Ghosh, R.; Meng, X.; Roy, A.; Kim, J.-S.; He, F.; Mason, S. C.; Xu, X.; Lin, J.-F.; Akinwande, D.; et al. Experimental evidence of exciton capture by mid-gap defects in CVD grown monolayer MoSe2. *NPJ. 2D Mater. Appl.* **2017**, *1*, 15.
(16) Harcourt, R. D.; Scholes, G. D.; Ghiggino, K. P. Rate expressions for excitation transfer. II. Electronic considerations of direct and through-configuration exciton resonance interactions. *J. Chem. Phys.* **1994**, *101*, 10521−10525.
(17) Yamagata, H.; Maxwell, D. S.; Fan, J.; Kittilstved, K. R.; Briseno, A. L.; Barnes, M. D.; Spano, F. C. HJ-aggregate behavior of crystalline 7,8,15,16-tetraazaterrylene: Introducing a new design paradigm for organic materials. *J. Phys. Chem. C* **2014**, *118*, 28842−28854.
(18) Hestand, N. J.; Tempelaar, R.; Knoester, J.; Jansen, T. L.; Spano, F. C. Exciton mobility control through sub-Å packing modifications in molecular crystals. *Phys. Rev. B* **2015**, *91*, 1−7.
(19) Krausko, J.; Malongwe, J. K.; Bičanová, G.; Klán, P.; Nachtigallová, D.; Heger, D. Spectroscopic Properties of Naphthalene on the Surface of Ice Grains Revisited: A Combined Experimental-Computational Approach. *J. Phys. Chem. A* **2015**, *119*, 8565−8578.
(20) Hsu, C. P.; You, Z. Q.; Chen, H. C. Characterization of the short-range couplings in excitation energy transfer. *J. Phys. Chem. C* **2008**, *112*, 1204−1212.
(21) Aragó, J.; Troisi, A. Dynamics of the Excitonic Coupling in Organic Crystals. *Phys. Rev. Lett.* **2015**, *114*, 026402.
(22) Eggeman, A. S.; Illig, S.; Troisi, A.; Sirringhaus, H.; Midgley, P. A. Measurement of molecular motion in organic semiconductors by thermal diffuse electron scattering. *Nat. Mater.* **2013**, *12*, 1045−1049.
(23) Aragó, J.; Troisi, A. Regimes of exciton transport in molecular crystals in the presence of dynamic disorder. *Adv. Funct. Mater.* **2016**, *26*, 2316−2325.
(24) Renaud, N.; Grozema, F. C. Intermolecular vibrational modes speed up singlet fission in perylenediimide crystals. *J. Phys. Chem. Lett.* **2015**, *6*, 360−365.
(25) Fratini, S.; Mayou, D.; Ciuchi, S. The transient localization scenario for charge transport in crystalline organic materials. *Adv. Funct. Mater.* **2016**, *26*, 2292−2315.
(26) Troisi, A.; Orlandi, G. Charge-transport regime of crystalline organic semiconductors: diffusion limited by thermal off-diagonal electronic disorder. *Phys. Rev. Lett.* **2006**, *96*, 086601.
(27) Rispens, M. T.; Meetsma, A.; Rittberger, R.; Brabec, C. J.; Sariciftci, N. S.; Hummelen, J. C. Influence of the solvent on the crystal structure of PCBM and the efficiency of MDMO-PPV:PCBM 'plastic' solar cells. *Chem. Commun.* **2003**, 2116−2118.
(28) Cheung, D. L.; Troisi, A. Theoretical Study of the Organic Photovoltaic Electron Acceptor PCBM: Morphology, Electronic Structure, and Charge Localization. *J. Phys. Chem. C* **2010**, *114*, 20479−20488.
(29) Reyes-Reyes, M.; Kim, K.; Dewald, J.; López-Sandoval, R.; Avadhanula, A.; Curran, S.; Carroll, D. L. Meso-structure formation for enhanced organic photovoltaic cells. *Org. Lett.* **2005**, *7*, 5749−5752.
(30) Heck, A.; Kranz, J. J.; Elstner, M. Simulation of temperature-dependent charge transport in organic semiconductors with various degrees of disorder. *J. Chem. Theory Comput.* **2016**, *12*, 3087−3096.
(31) Giannini, S.; Carof, A.; Ellis, M.; Yang, H.; Ziogos, O. G.; Ghosh, S.; Blumberger, J. Quantum localization and delocalization of charge carriers in organic semiconducting crystals. *Nat. Commun.* **2019**, *10*, 3843.
(32) Peng, W.-T.; Brey, D.; Giannini, S.; Dell'Angelo, D.; Burghardt, I.; Blumberger, J. Exciton Dissociation in a Model Organic Interface: Excitonic State-Based Surface Hopping versus Multiconfigurational Time-Dependent Hartree. *J. Phys. Chem. Lett.* **2022**, *13*, 7105−7112.
(33) Giannini, S.; Peng, W.-T.; Cupellini, L.; Padula, D.; Carof, A.; Blumberger, J. Exciton transport in molecular organic semiconductors boosted by transient quantum delocalization. *Nat. Commun.* **2022**, *13*, 2755.
(34) Menke, S. M.; Holmes, R. J. Exciton diffusion in organic photovoltaic cells. *Energy Environ. Sci.* **2014**, *7*, 499−512.
(35) Mikhnenko, O. V.; Blom, P. W.; Nguyen, T.-Q. Exciton diffusion in organic semiconductors. *Energy Environ. Sci.* **2015**, *8*, 1867−1888.
(36) Dostál, J.; Fennel, F.; Koch, F.; Herbst, S.; Würthner, F.; Brixner, T. Direct observation of exciton-exciton interactions. *Nat. Commun.* **2018**, *9*, 1−8.
(37) Roy, P.; Bressan, G.; Gretton, J.; Cammidge, A. N.; Meech, S. R. Ultrafast Excimer Formation and Solvent Controlled Symmetry Breaking Charge Separation in the Excitonically Coupled Subphthalocyanine Dimer. *Angew. Chem., Int. Ed.* **2021**, *60*, 10568−10572.
(38) Kubo, T.; Häusermann, R.; Tsurumi, J.; Soeda, J.; Okada, Y.; Yamashita, Y.; Akamatsu, N.; Shishido, A.; Mitsui, C.; Okamoto, T.; et al. Suppressing molecular vibrations in organic semiconductors by inducing strain. *Nat. Commun.* **2016**, *7*, 1−7.
(39) Chandran, D.; Lee, K. S. Diketopyrrolopyrrole: A versatile building block for organic photovoltaic materials. *Macromol. Res.* **2013**, *21*, 272−283.

https://doi.org/10.1021/acs.jpcc.2c07984
J. Phys. Chem. C XXXX, XXX, XXX−XXX

(40) Naik, M. A.; Patil, S. Diketopyrrolopyrrole-based conjugated polymers and small molecules for organic ambipolar transistors and solar cells. *J. Polym. Sci. Part A Polym. Chem.* **2013**, *51*, 4241−4260.
(41) Kaur, M.; Choi, D. H. Diketopyrrolopyrrole: Brilliant red pigment dye-based fluorescent probes and their applications. *Chem. Soc. Rev.* **2015**, *44*, 58−77.
(42) Li, Y.; Sonar, P.; Murphy, L.; Hong, W. High mobility diketopyrrolopyrrole (DPP)-based organic semiconductor materials for organic thin film transistors and photovoltaics. *Energy Environ. Sci.* **2013**, *6*, 1684.
(43) Pop, F.; Lewis, W.; Amabilino, D. B. Solid state supramolecular structure of diketopyrrolopyrrole chromophores: Correlating stacking geometry with visible light absorption. *CrystEngComm* **2016**, *18*, 8933−8943.
(44) Fratini, S.; Nikolka, M.; Salleo, A.; Schweicher, G.; Sirringhaus, H. Charge transport in high-mobility conjugated polymers and molecular semiconductors. *Nat. Mater.* **2020**, *19*, 491−502.
(45) Jiang, L.; Hirst, J. D.; Do, H. Structure-Property Relationships in Amorphous Thieno [3, 2-b] thiophene-Diketopyrrolopyrrole-Thiophene-Containing Polymers. *J. Phys. Chem. C* **2022**, *126*, 10842−10854.
(46) Naik, M. A.; Venkatramaiah, N.; Kanimozhi, C.; Patil, S. Influence of side-chain on structural order and photophysical properties in thiophene based diketopyrrolopyrroles: A systematic study. *J. Phys. Chem. C* **2012**, *116*, 26128−26137.
(47) Hartnett, P. E.; Margulies, E. A.; Mauck, C. M.; Miller, S. A.; Wu, Y.; Wu, Y.-L.; Marks, T. J.; Wasielewski, M. R. Effects of Crystal Morphology on Singlet Exciton Fission in Diketopyrrolopyrrole Thin Films. *J. Phys. Chem. B* **2016**, *120*, 1357−1366.
(48) Jiang, L.; Rogers, D. M.; Hirst, J. D.; Do, H. Force Fields for Macromolecular Assemblies Containing Diketopyrrolopyrrole and Thiophene. *J. Chem. Theory Comput.* **2020**, *16*, 5150−5162.
(49) Kunsel, T.; Jansen, T. L. C.; Knoester, J. Scaling relations of exciton diffusion in linear aggregates with static and dynamic disorder. *J. Chem. Phys.* **2021**, *155*, 134305.
(50) Ghosh, R.; Spano, F. C. Excitons and Polarons in Organic Materials. *Acc. Chem. Res.* **2020**, *53*, 2201−2211.
(51) Fornari, R. P.; Aragó, J.; Troisi, A. Exciton dynamics in phthalocyanine molecular crystals. *J. Phys. Chem. C* **2016**, *120*, 7987−7996.
(52) Strong, S. E.; Hestand, N. J. Modeling nonlocal electron-phonon coupling in organic crystals using interpolative maps: The spectroscopy of crystalline pentacene and 7, 8, 15, 16-tetraazaterrylene. *J. Chem. Phys.* **2020**, *153*, 124113.
(53) Troisi, A.; Orlandi, G. Dynamics of the intermolecular transfer integral in crystalline organic semiconductors. *J. Phys. Chem. A* **2006**, *110*, 4065−4070.
(54) Troisi, A. Prediction of the absolute charge mobility of molecular semiconductors: the case of rubrene. *Adv. Mater.* **2007**, *19*, 2000−2004.
(55) Do, H.; Troisi, A. Developing accurate molecular mechanics force fields for conjugated molecular systems. *Phys. Chem. Chem. Phys.* **2015**, *17*, 25123−25132.
(56) Chai, J.-D.; Head-Gordon, M. Long-range corrected hybrid density functionals with damped atom-atom dispersion corrections. *Phys. Chem. Chem. Phys.* **2008**, *10*, 6615−6620.
(57) Frisch, M. J. et al. *Gaussian 16, Revision C.01*; Gaussian, Inc.: Wallingford, CT, 2016.
(58) Dodda, L. S.; de Vaca, I. C.; Tirado-Rives, J.; Jorgensen, W. L. LigParGen web server: An automatic OPLS-AA parameter generator for organic ligands. *Nucleic Acids Res.* **2017**, *45*, W331−W336.
(59) Phillips, J. C.; Braun, R.; Wang, W.; Gumbart, J.; Tajkhorshid, E.; Villa, E.; Chipot, C.; Skeel, R. D.; Kalé, L.; Schulten, K. Scalable molecular dynamics with NAMD. *J. Comput. Chem.* **2005**, *26*, 1781−1802.
(60) Hoover, W. G.; Ladd, A. J. C.; Moran, B. High-Strain-Rate Plastic Flow Studied via Nonequilibrium Molecular Dynamics. *Phys. Rev. Lett.* **1982**, *48*, 1818−1820.
(61) Herce, H. D.; Garcia, A. E.; Darden, T. The Electrostatic Surface Term: (I) Periodic Systems. *J. Chem. Phys.* **2007**, *126*, 124106.
(62) Lu, T.; Chen, F. Multiwfn: a multifunctional wavefunction analyzer. *J. Comput. Chem.* **2012**, *33*, 580−592.
(63) Aragó, J.; Troisi, A. Excitonic couplings between molecular crystal pairs by a multistate approximation. *J. Chem. Phys.* **2015**, *142*, 164107.
(64) Bondarenko, A. S.; Knoester, J.; Jansen, T. L. Comparison of methods to study excitation energy transfer in molecular multi-chromophoric systems. *Chem. Phys.* **2020**, *529*, 110478.
(65) Li, X.; Buda, F.; de Groot, H. J.; Sevink, G. A. Dynamic Disorder Drives Exciton Transfer in Tubular Chlorosomal Assemblies. *J. Phys. Chem. B* **2020**, *124*, 4026−4035.
(66) Johansson, J. R.; Nation, P. D.; Nori, F. QuTiP: An open-source Python framework for the dynamics of open quantum systems. *Comput. Phys. Commun.* **2012**, *183*, 1760−1772.
(67) Johansson, J.; Nation, P. D.; Nori, F. QuTiP 2: A Python framework for the dynamics of open quantum systems. *Comput. Phys. Commun.* **2013**, *184*, 1234−1240.
(68) Dhar, J.; Karothu, D. P.; Patil, S. Herringbone to cofacial solid state packing via H-bonding in diketopyrrolopyrrole (DPP) based molecular crystals: influence on charge transport. *Chem. Commun.* **2015**, *51*, 97−100.
(69) Fassioli, F.; Dinshaw, R.; Arpin, P. C.; Scholes, G. D. Photosynthetic light harvesting: excitons and coherence. *J. R. Soc. Interface* **2014**, *11*, 20130901.
(70) Aragó, J.; Viruela, P. M.; Gierschner, J.; Ortí, E.; Milián-Medina, B. Oligothienoacenes versus oligothiophenes: impact of ring fusion on the optical properties. *Phys. Chem. Chem. Phys.* **2011**, *13*, 1457−1465.
(71) Hestand, N. J.; Kazantsev, R. V.; Weingarten, A. S.; Palmer, L. C.; Stupp, S. I.; Spano, F. C. Extended-charge-transfer excitons in crystalline supramolecular photocatalytic scaffolds. *J. Am. Chem. Soc.* **2016**, *138*, 11762−11774.
(72) Van der Horst, J.-W.; Bobbert, P. A.; Michels, M. A.; Bässler, H. Calculation of excitonic properties of conjugated polymers using the Bethe-Salpeter equation. *J. Chem. Phys.* **2001**, *114*, 6950−6957.
(73) Knupfer, M. Exciton binding energies in organic semiconductors. *Appl. Phys. A: Mater. Sci. Process.* **2003**, *77*, 623−626.
(74) Hummer, K.; Ambrosch-Draxl, C. Oligoacene exciton binding energies: Their dependence on molecular size. *Phys, Rev. B* **2005**, *71*, 081202.
(75) Seitz, M.; Magdaleno, A. J.; Alcázar-Cano, N.; Meléndez, M.; Lubbers, T. J.; Walraven, S. W.; Pakdel, S.; Prada, E.; Delgado-Buscalioni, R.; Prins, F. Exciton diffusion in two-dimensional metal-halide perovskites. *Nat. Commun.* **2020**, *11*, 1−8.
(76) Carof, A.; Giannini, S.; Blumberger, J. How to calculate charge mobility in molecular materials from surface hopping non-adiabatic molecular dynamics-beyond the hopping/band paradigm. *Phys. Chem. Chem. Phys.* **2019**, *21*, 26368−26386.
(77) Xie, W.; Holub, D.; Kubar, T.; Elstner, M. Performance of Mixed Quantum-Classical Approaches on Modeling the Crossover from Hopping to Bandlike Charge Transport in Organic Semiconductors. *J. Chem. Theory Comput.* **2020**, *16*, 2071−2084.
(78) Huijser, A.; Savenije, T. J.; Meskers, S. C.; Vermeulen, M. J.; Siebbeles, L. D. The mechanism of long-range exciton diffusion in a nematically organized porphyrin layer. *J. Am. Chem. Soc.* **2008**, *130*, 12496−12500.
(79) Li, X.; Buda, F.; De Groot, H. J.; Sevink, G. J. Dynamic Disorder Drives Exciton Transfer in Tubular Chlorosomal Assemblies. *J. Phys. Chem. B* **2020**, *124*, 4026−4035.
(80) Chenu, A.; Scholes, G. D. Coherence in energy transfer and photosynthesis. *Annu. Rev. Phys. Chem.* **2015**, *66*, 69−96.

https://doi.org/10.1021/acs.jpcc.2c07984
J. Phys. Chem. C XXXX, XXX, XXX−XXX